scientific reports

Check for updates

OPEN

Luminescent materials with dual-mode excitation and tunable emission color for anti-counterfeiting applications

Nina Jaroch[1], Justyna Czajka[2] & Agata Szczeszak[1]✉

$GdVO_4$-based dual-mode phosphors were successfully synthesized via a hydrothermal approach. The X-ray diffraction analysis determined the tetragonal structure as well as $I4_1/amd$ space group of products by comparing with a reference pattern no. ICDD #01-072-0277. The morphology of yielded phosphors was confirmed by transmission electron microscopy and scanning electron microscopy. Detailed spectroscopy analysis revealed tunable luminescence properties with an increasing Yb^{3+} content in series of $GdVO_4$: x% Yb^{3+}, y% Tm^{3+}, 5% Eu^{3+} (x = 5, 10, 15, 20; y = 0.1, 0.5, 1) phosphors. For Yb^{3+}, Tm^{3+}, and Eu^{3+}- codoped phosphors we observed bands related to the $^1G_4 \rightarrow {}^3H_6$ and $^1G_4 \rightarrow {}^3F_4$ transitions of Tm^{3+} ions, occurred through the cooperative up-conversion mechanism, where two nearby Yb^{3+} ions were involved in near-infrared absorption. Moreover, the $GdVO_4$: 20% Yb^{3+}, 0.5% Tm^{3+}, 5% Eu^{3+} showed the most outstanding color tunability from red color (x = 0.6338, y = 0.3172) under UV to blue color (x = 0.2640, y = 0.1988) under NIR excitation, which can be applied in anti-counterfeiting activity.

Inorganic materials doped with lanthanide ions (Ln^{3+}) play a significant role in many fields of everyday life, based on their numerous applications as lasers, thin film phosphors, in drug delivery, bioimaging, or anti-counterfeiting[1–7]. The last-mentioned group consists of several media in which anti-counterfeiting tags are implemented, such as bar codes, inks, holograms, RFID (Radio Frequency Identification). Every aforementioned security approach has its limitations and thus cannot be applied in i.e., clothes or document markings, which may be regularly treated with water, washing agents, or UV radiation. Recently developed cellulose fibers modified- with inorganic phosphors[8–12] are prepared via an environmentally friendly NMMO (N-Methylmorpholine-N-Oxide) method. As an outcome, the so-called Tencel fibers may be used for paper modification or as a part of the fabric. Also, during this rigorous process of fibers preparation, the luminescent modifier used has to outstand with its excellent stability. In our research, we chose $GdVO_4$-based dual-mode phosphors based on their strong energy absorption as well as the high efficiency of energy transfer processes[13–15]. Another advantage of vanadate-based phosphors as an alternative type of material versus fluoride-based phosphors is their high thermal stability, beneficial in i.e. light-emitting diode application, in which operating temperature exceeds 100 °C[16]. In comparison to the vanadate materials, commonly used in phosphor applications fluoride materials are not only sensitive to high temperatures but also to surface contamination which may accidentally influence spectroscopic properties such as luminescence lifetime or emission color[17].

Contrary to the accidental influence, the intentional impact on the intensity and different luminescence color under UV or NIR excitation is caused by the specified Ln^{3+} dopant concentration. Rare earth-doped materials exhibiting dual-mode luminescence possess vast potential for various applications[18–21]. When a combination of ions capable of absorbing energy with diverse energy values based on their electron structure is used, a unique luminescence color tunability can be achieved. The perfect combination for obtaining tunable luminescence is the system comprising Yb^{3+}, Tm^{3+}, and Eu^{3+} ions. Here, the NIR excitation of 980 nm can be absorbed by Yb^{3+} and after transferring two or more photons towards Tm^{3+} and Eu^{3+} ions, a visible up-conversion emission is observed, which is highly dependent on Tm^{3+} and Eu^{3+} ratio. Also, under UV irradiation, there is a possibility of direct Eu^{3+} excitation or energy transfer from the orthovanadate matrix to dopant ions—in both cases, a red emission associated with Eu^{3+} is observed[22,23].

[1]Faculty of Chemistry, Adam Mickiewicz University, Poznań, Uniwersytetu Poznańskiego 8, 61-614 Poznań, Poland. [2]Faculty of Chemical Technology and Engineering, Bydgoszcz University of Science and Technology, Seminaryjna 3, 85-326 Bydgoszcz, Poland. ✉email: agata_is@amu.edu.pl

In this study, we aim to provide a comprehensive understanding of the properties and applications of the luminescent marks based on doped orthovanadates. All of above-mentioned features of the $GdVO_4$: Yb^{3+}, Tm^{3+}, Eu^{3+} phosphors synthesized by the feasible hydrothermal approach, designate as perfect for the anti-counterfeiting applications as the color tunability within the same material is difficult to falsify. The study introduces dual-mode orthovanadates as a viable substitute for fluoride-based materials in the realm of anti-counterfeiting tags. Through precise selection of dopant ions and host matrix, the resulting luminophores undergo up-conversion processes and demonstrate robust emission capabilities owing to charge transfer phenomena between O^{2-} and Eu^{3+} ions. These distinct mechanisms give rise to diverse color emissions and various wavelength excitation. Moreover, the orthovanadate materials exhibit remarkable resilience to harsh environmental conditions, including elevated temperatures, thereby rendering them advantageous by comparison to the aforementioned fluorides, which are more prone to decomposition.

A potential application of the implementation of a orthovanadates modifier into cellulose fibers for paper and fabric markings has been confirmed by the patent application submitted[43,44]. By showcasing the real-world application of our material, we establish its potential for practical implementation and highlight its relevance to various industries. Finally, according to our knowledge, this is the first time that Yb^{3+}, Tm^{3+}, Eu^{3+} dopants are incorporated into the orthovanadate matrix, and its structural followed by spectroscopic properties are determined. It fills a gap in the existing literature by presenting an innovative approach that has practical implications and opens new avenues for future research and development.

Experimental section

Materials. Ammonium metavanadate (NH_4VO_3, Sigma Aldrich, 99.9%), gadolinium(III) oxide (Gd_2O_3, Standford Materials, 99.99%), ytterbium(III) oxide (Yb_2O_3, Standford Materials, 99.99%), thulium(III) oxide (Tm_2O_3, Standford Materials, 99.99%), europium(III) oxide (Standford Materials, 99.99%) and acetic acid (CH_3COOH, POCH, 99,95%) used in the synthesis of the materials.

Methods. A series of $GdVO_4$: x% Yb^{3+}, y% Tm^{3+}, 5% Eu^{3+} (x = 5, 10, 15, 20; y = 0.1, 0.5, 1) was obtained in hydrothermal conditions. The concentration and the type of dopants was altered based on our knowledge and the literature in order to observe efficient emission processes[24–28]. In addition, the concentration of Yb^{3+}, Tm^{3+} and Eu^{3+} dopant ions in prominent $GdVO_4$ host was altered to provide the intense, dual-mode luminescence under UV and NIR irradiation for anticounterfeiting applications. The composition of Ln^{3+} ions used was selected to ensure the emission color dependent on excitation wavelength thus considered material is more difficult to replicate.

The synthesis was performed in Berghof autoclave (max. pressure 200 bar, additional stirring). All of the substrates were used as water solutions. The stoichiometric combination of 0.25 M $Ln(CH_3COO)_3$ was mixed with the 0.1 M NH_4VO_3 added dropwise under continuous stirring for 30 min. Resultant transparent mixture (pH 4.7) was then transferred to Teflon vessel and put for hydrothermal process under 180 °C for 3 h which yielded with yellow powder. Next, when the autoclave was naturally cooled to room temperature, the product was collected by centrifugation, washed with 1:1 mixture of deionized water and ethanol. Finally, the product was dried at 80°C for 24 h for further analysis.

Characterization. The structural analysis was conducted with Bruker AXS D8 Advance powder X-ray diffractometer equipped with Johansson's monochromator and Lynx Eye strip detector, whereas the measurements were performed with Cu-$K_\alpha 1$ $\lambda = 15{,}418$ Å radiation within the 10–60 2Θ range, 0.05°/s step size. Morphology of studied materials was investigated with the use of transmission electron microscopy, TEM (JEOL 1400 with acceleration voltage of 80 kV) as well as scanning electron microscopy, SEM (Quanta 250 FEG, FEI equipped with EDAX detector). Luminescence properties were studied in terms of photoluminescence and upconversion luminescence, i.e. under UV or NIR excitation. The former was studied with the use of Hitachi F-7000 spectrofluorimeter, equipped with xenon lamp excitation source. The latter phenomenon was studied in terms of emission, luminescence decay and the number of photons involved in the process, with the use of PIXIS:256E Digital CCD Camera equipped with SP-2156 Imaging Spectrograph (Princeton Instruments), Mixed Domain Oscilloscope—200 MHz—Tektronix MDO3022 as well as the excitation source of CNI NIR 2W LASER 975 nm. All of the spectroscopic measurements were conducted at 293 K.

Results and discussion

Structure and morphology. Behind every specific luminescence feature, there are structural and morphological reasons as well. As seen in Fig. 1, the replacement of 25.5% of Gd^{3+} ions with dopant ions in the host structure did not cause severe lattice distortions since the ionic radius of Eu^{3+} is similar, while the Yb^{3+} and Tm^{3+} radii are smaller than the one of Gd^{3+}[29]. The synthesized compounds are confirmed to be of $GdVO_4$ $I4_1/amd$ tetragonal zircon-type ($ZrSiO_4$) structure with the cell parameters of a = b = 7.2126 Å, c = 6.3483 Å, according to the reference pattern no. ICDD #01-072-0277[30,31]. The tetragonal and polyhedral structure of $GdVO_4$ are presented in Fig. 2c. Here, vanadium atom of $[VO_4]^{3-}$ is tetrahedrally coordinated with O^{2-} ions, whereas the Ln^{3+} are surrounded by eight oxygen atoms in a distorted dodecahedron structure[32]. The presence of sharp, narrow reflexes indicates discussed materials as highly crystalline and bulk. By the fact that none of the additional peaks are observed, synthesized powders are monophased and the replacement of Gd^{3+} by Ln^{3+} dopants was successful. What has to be said, an increased grain size growth as well as excellent crystallinity are caused by inevitable high temperature annealing (900 °C) which was applied to induce the UC luminescence, initially diminished by structure defects, typical for materials synthesized in hydrothermal conditions[33]. These features were further confirmed with the use of TEM and SEM methods (Fig. 2a,b). The obtained orthovanadate crystals were

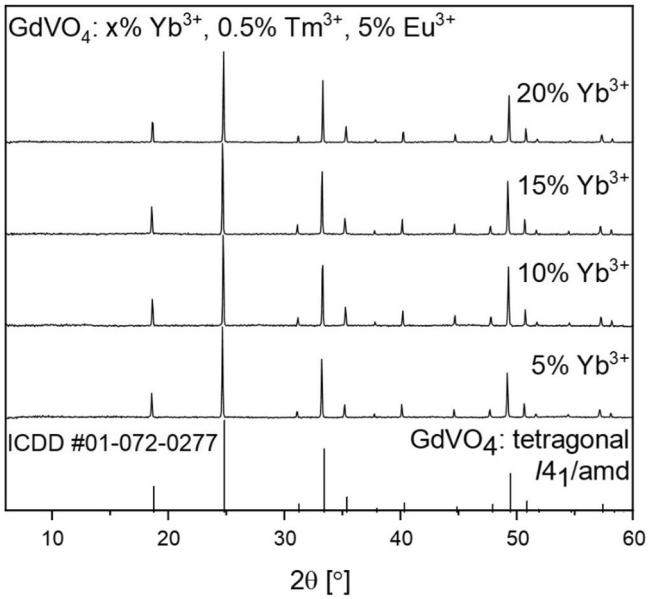

Figure 1. A set of diffraction data for $GdVO_4$: x% Yb^{3+}, 0.5% Tm^{3+}, 5% Eu^{3+} materials.

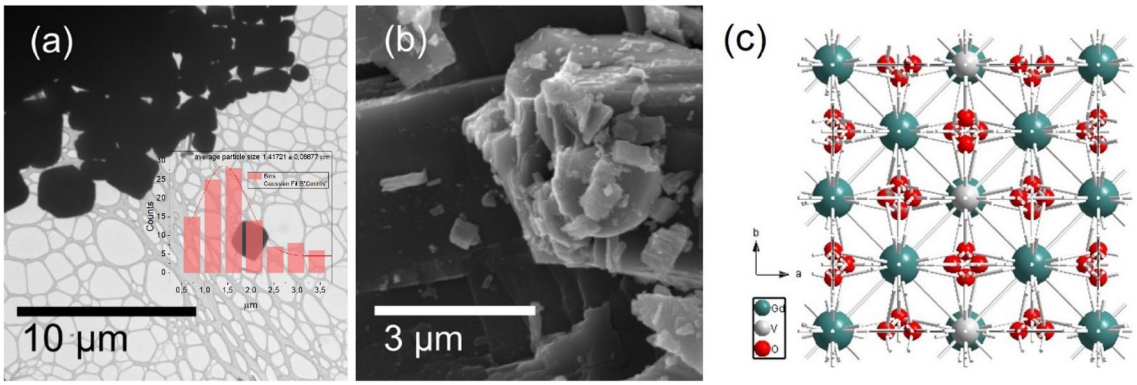

Figure 2. Morphology representation of $GdVO_4$: 20% Yb^{3+}, 0.5% Tm^{3+}, 5% Eu^{3+} sample in terms of TEM with histogram presenting size distribution (**a**) and SEM (**b**) methods and crystal structure of $GdVO_4$ $I4_1/amd$ tetragonal zircontype ($ZrSiO_4$) (**c**).

observed to be agglomerated, displaying an irregular morphology. The average grain size, determined from the broadest fraction, was found to be approximately 1.5 µm. These observations confirm the microstructural properties of the orthovanadate crystals and provide quantitative data regarding their size distribution illustrated on histogram (inset Fig. 2a). Despite the large grain size, it was possible to disperse the powder in water for further use in cellulose fiber modification.

Spectroscopic properties. According to the Figs. 3 and 4, $GdVO_4$: 20% Yb^{3+}, 0.5% Tm^{3+}, 5% Eu^{3+} sample was chosen amongst the series as the most promising sample thus used for the fabric preparation based not only on its diverse luminescence color under UV and NIR excitation, but also the outstanding UC emission in the visible range.

Photoluminescence. Based on the excitation spectrum in the UV range Fig. 4, the O^{2-}–Eu^{3+} charge transfer band (CT) with the maximum at 310 nm was chosen to observe visible luminescence at 621 nm, assigned to the $^5D_0 \rightarrow {}^7F_2$ transition. What has to be mentioned, the broad CT band is in fact combined of O^{2-}–V^{5+} and O^{2-}–Eu^{3+}; however, based on the small difference in between O^{2-} and V^{5+}, as well as the large charge difference, O^{2-}–V^{5+} in $[VO_4]^{3-}$ is easier observed[34]. Also, there are additional weak f–f transitions typical for Eu^{3+} ions in the 200–500 nm range[35,36]. Based on the ionic radii difference[34], Gd^{3+} is being replaced by Eu^{3+} thus in the $GdVO_4$: Yb, Eu, Tm system, Eu^{3+} has D_{2d} symmetry as it is surrounded by eight O^{2-} ions. Relative intensity of $^5D_0 \rightarrow {}^7F_1$ and $^5D_0 \rightarrow {}^7F_2$ is altered based on the local site symmetry of the Eu^{3+} ions[11,37,38]. In this research, the intensity of hypersensitive $^5D_0 \rightarrow {}^7F_2$ is the highest among the Eu^{3+} emission bands which indicated the low symmetry around Eu^{3+} ions[38]. What is more, with an increasing Yb^{3+} concentration, the intensity of both excitation and

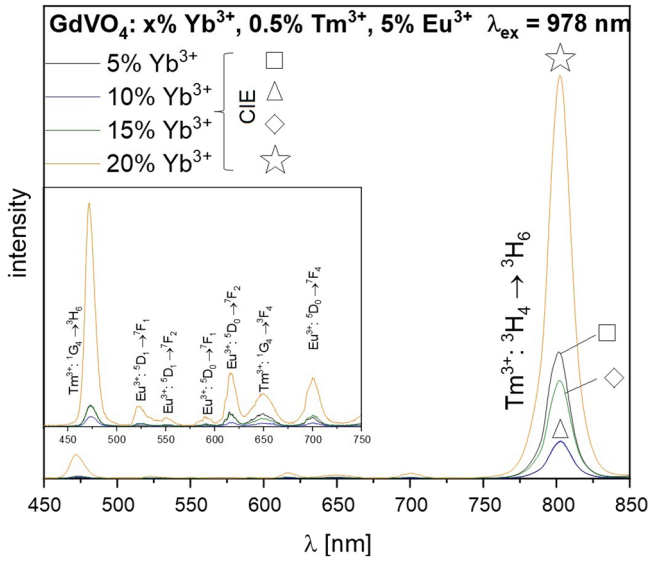

Figure 3. UC luminescence spectra for $GdVO_4$: x% Yb^{3+}, 0.5% Tm^{3+}, 5% Eu^{3+} samples recorded under CW 975 nm excitation.

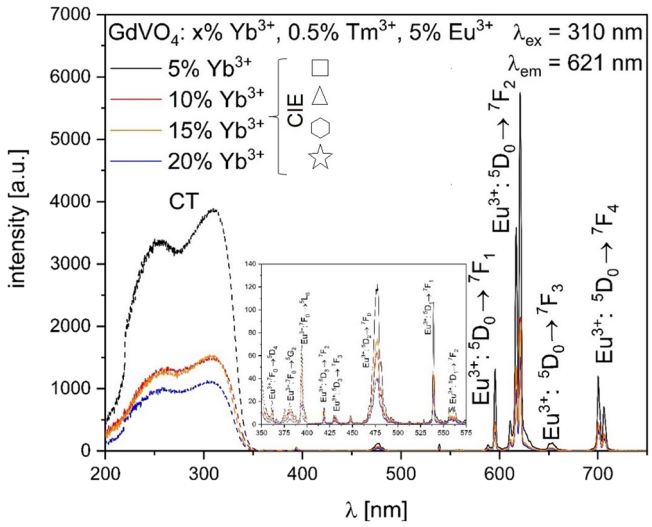

Figure 4. PLE (dashed line) and PL (solid line) spectra of $GdVO_4$:x%Yb^{3+}, 0.5%Tm^{3+}, 5%Eu^{3+} materials.

emission curves is decreasing in terms of the $Eu^{3+} \rightarrow Yb^{3+}$ energy transfer, since the distance between these ions is shortened[38]. This phenomenon is further confirmed by the calculated Eu^{3+} luminescence lifetime values (Table 1) monitored under 310 nm excitation. With the increasing Yb^{3+} concentration, the energy is migrating from Eu^{3+} excited states to Yb^{3+} ions.

According to the chromaticity diagram Fig. 5, under 310 nm excitation the outcoming luminescence color is not altered by the incorporated Tm^{3+} ions.

Upconversion luminescence. It is essential for dual-mode luminescence (ergo inimitable anti-counterfeiting materials) to be intense both under UV and NIR irradiation. According to the upconversion spectrum depicted in Fig. 4, the energy transfer between Eu^{3+} and Tm^{3+} ions is observed as variety of Eu^{3+} and Tm^{3+} emission bands are present in the spectrum. What has to be noted, the population of Eu^{3+} via inefficient phonon-assisted- Yb^{3+}–Eu^{3+} is barely observed; here, Tm^{3+} acts as an energy mediator between the sensitizer (Yb^{3+}) and emitter (Eu^{3+})[22]. According to that, several emission bands associated to the Tm^{3+} and Eu^{3+} are observed in the spectrum, which vary with intensity, namely $^1G_4 \rightarrow {}^3H_6$ (Tm^{3+}, ~ 478 nm), $^5D_1 \rightarrow {}^7F_1$ (Eu^{3+}, ~ 521 nm), $^5D_1 \rightarrow {}^7F_2$ (Eu^{3+}, ~ 552 nm), $^5D_0 \rightarrow {}^7F_1$ (Eu^{3+}, ~ 590 nm), $^5D_0 \rightarrow {}^7F_2$ (Eu^{3+}, ~ 615 nm), $^1G_4 \rightarrow {}^3F_4$ (Tm^{3+}, ~ 650 nm), $^5D_0 \rightarrow {}^7F_4$ (Eu^{3+}, ~ 700 nm) as well as the most intense $^3H_4 \rightarrow {}^3H_6$ (Tm^{3+}, ~ 800 nm) band. The last-mentioned transition is observed in NIR region of spectrum thus it does not influence the emission color. What has to be mentioned,

Luminescence lifetime [μs]					
Sample	Eu^{3+}: $^5D_2 \rightarrow {}^7F_0$ (~476 nm)	Eu^{3+}: $^5D_0 \rightarrow {}^7F_1$ (~596 nm)	Eu^{3+}: $^5D_0 \rightarrow {}^7F_2$ (~621 nm)	Eu^{3+}: $^5D_0 \rightarrow {}^7F_3$ (~654 nm)	Eu^{3+}: $^5D_0 \rightarrow {}^7F_4$ (~700 nm)
$GdVO_4$: 5% Yb^{3+}, 0.5% Tm^{3+}, 5% Eu^{3+}	171 ± 5	342 ± 5	282 ± 2	347 ± 6	289 ± 1
$GdVO_4$: 10% Yb^{3+}, 0.5% Tm^{3+}, 5% Eu^{3+}	176 ± 5	285 ± 2	306 ± 3	308 ± 3	280 ± 2
$GdVO_4$: 15% Yb^{3+}, 0.5% Tm^{3+}, 5% Eu^{3+}	176 ± 5	318 ± 5	296 ± 4	320 ± 6	260 ± 2
$GdVO_4$: 20% Yb^{3+}, 0.5% Tm^{3+}, 5% Eu^{3+}	175 ± 5	298 ± 5	281 ± 3	325 ± 7	171 ± 5

Table 1. A set of calculated luminescence lifetime values for $GdVO_4$: x% Yb^{3+}, 0.5% Tm^{3+}, 5% Eu^{3+} phosphors under 310 nm excitation.

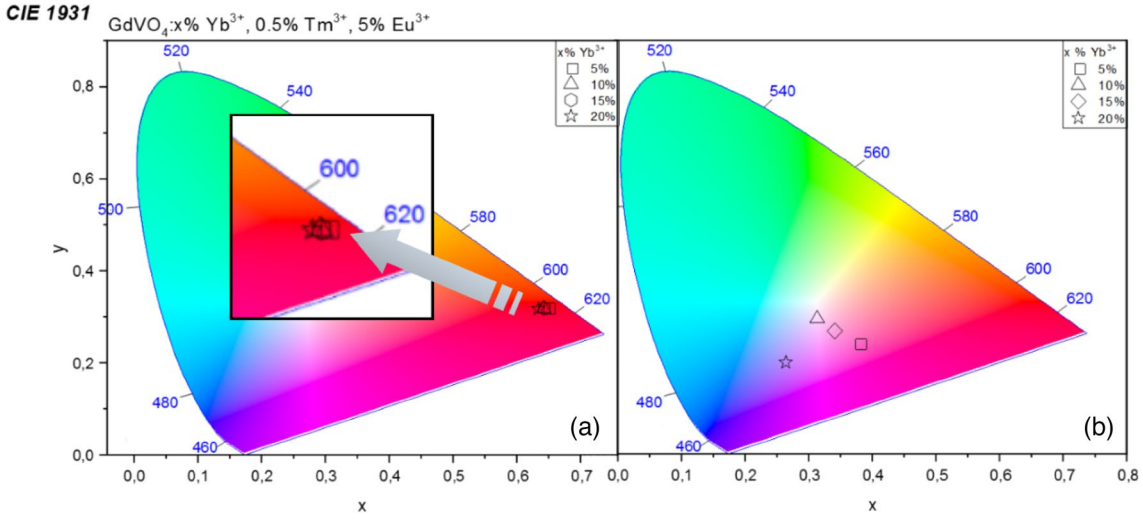

Figure 5. Chromaticity diagram for $GdVO_4$: x% Yb^{3+}, 0.5% Tm^{3+}, 5% Eu^{3+} samples under 310 nm with an enlarged inset (**a**) and CW 975 nm excitation (**b**).

throughout changing Yb^{3+} concentration, the chromaticity coordinates of synthesized materials change, according to the Fig. 5 and Table 2. With an increasing Yb^{3+} content, the luminescence color shifts from the red towards purple and blue region of CIE chromaticity diagram. By the gradual substitution of Gd^{3+} by Yb^{3+}, the distance between sensitizer and emitters such as Tm^{3+}, Eu^{3+} decrease. As mentioned before, the efficiency of Yb^{3+}–Eu^{3+} transfer is low thus the Yb^{3+}–Tm^{3+} transfer is favored here. In this case, the competitive Tm^{3+}–Eu^{3+} absorption is decreased, which is also connected with the lower intensity of Eu^{3+} emission bands in the UC spectrum, as well as the red component of the luminescence color[23]. Also, when Yb^{3+}–Tm^{3+} is greatly enhanced, the relative intensity between blue and red emissions of Tm^{3+} is increased, which results with the outcoming blue upconversion luminescence[40,41].

The population of Eu^{3+} and Tm^{3+} excited levels, as well as the energy transfer between these species were studied in terms of luminescence decay. Here, due to the color change, the most important bands are the ones in the blue and red region of spectrum. Based on that, the greatest attention was put to the lifetime of $^1G_4 \rightarrow {}^3H_6$ (Tm^{3+}, ~ 478 nm), $^5D_0 \rightarrow {}^7F_2$ (Eu^{3+}, ~ 615 nm) and $^1G_4 \rightarrow {}^3F_4$ (Tm^{3+}, ~ 650 nm). As shown in Table 3, the luminescence lifetime of Eu^{3+} is decreasing with an increasing Yb^{3+} content. Based on that, the possibility of Tm^{3+}–Eu^{3+} is diminished, whereas Yb^{3+}–Tm^{3+} transfer is favored. It is also confirmed by the enhanced blue emission of Tm^{3+} since less energy is transferred towards Eu^{3+} site of lattice. Moreover, in order to derive the average number of

	Chromaticity coordinates (x, y)	
Sample	UV	NIR
$GdVO_4$: 5% Yb^{3+}, 0.5% Tm^{3+}, 5% Eu^{3+}	0.6495, 0.3202	0.3808, 0.2418
$GdVO_4$: 10% Yb^{3+}, 0.5% Tm^{3+}, 5% Eu^3	0.6424, 0.3183	0.3134, 0.2942
$GdVO_4$: 15% Yb^{3+}, 0.5% Tm^{3+}, 5% Eu^{3+}	0.6431, 0.3181	0.3411, 0.2672
$GdVO_4$: 20% Yb^{3+}, 0.5% Tm^{3+}, 5% Eu^{3+}	0.6338, 0.3172	0.2640, 0.1988

Table 2. A set of calculated chromaticity coordinates (x,y) for $GdVO_4$: x% Yb^{3+}, 0.5% Tm^{3+}, 5% Eu^{3+} phosphors under 310 nm and 975 nm excitation.

Luminescence lifetime [μs]						
Sample	Tm^{3+}: $^1G_4 \rightarrow {}^3H_6$ (~476 nm)	Eu^{3+}: $^5D_1 \rightarrow {}^7F_1$ (~521 nm)	Eu^{3+}: $^5D_0 \rightarrow {}^7F_2$ (~615 nm)	Tm^{3+}: $^1G_4 \rightarrow {}^3F_4$ (~650 nm)	Eu^{3+}: $^5D_0 \rightarrow {}^7F_4$ (~700 nm)	Tm^{3+}: $^3H_4 \rightarrow {}^3H_6$ (~800 nm)
$GdVO_4$: 5% Yb^{3+}, 0.5% Tm^{3+}, 5% Eu^{3+}	85 ± 5	88 ± 2	229 ± 5	99 ± 5	442 ± 1	88 ± 3
$GdVO_4$: 10% Yb^{3+}, 0.5% Tm^{3+}, 5% Eu^{3+}	89 ± 2	81 ± 5	225 ± 3	87 ± 3	204 ± 2	89 ± 2
$GdVO_4$: 15% Yb^{3+}, 0.5% Tm^{3+}, 5% Eu^{3+}	92 ± 2	98 ± 2	207 ± 4	97 ± 6	93 ± 2	88 ± 2
$GdVO_4$: 20% Yb^{3+}, 0.5% Tm^{3+}, 5% Eu^{3+}	95 ± 1	85 ± 2	180 ± 3	95 ± 1	158 ± 1	91 ± 1

Table 3. A set of calculated luminescence lifetime values for GdVO4: x% Yb^{3+}, 0.5% Tm^{3+}, 5% Eu^{3+} phosphors under 975 nm excitation.

photons (n) involved in the upconversion process, a laser power dependent luminescence study was performed (Fig. 6). Interestingly, the slopes (n) of $^1G_4 \rightarrow {}^3H_6$ and $^1G_4 \rightarrow {}^3F_4$ transitions suggest the involvement of two photons regardless the Yb^{3+} concentration. In the contrary to the common understanding of the $^1G_4$ population mechanism, i.e. through threephoton- absorption, meant also as sequential sensitization, in the case of $GdVO_4$: x% Yb^{3+}, 0.5% Tm^{3+}, 5% Eu^{3+} a cooperative sensitization is in fact happening. In this mechanism there are two Yb^{3+} ions involved, which absorbs photons in order to promote themselves towards $^2F_{5/2}$ excited state. Then, a coupled cluster state of two Yb^{3+} ions formed transfers energy towards Tm^{3+} which results with the population of its $^1G_4$ level[42].

To summarize all studied processes, a mechanism of upconversion in $GdVO_4$: x% Yb^{3+}, 0.5% Tm^{3+}, 5% Eu^{3+} systems can be proposed in Fig. 7. The whole phenomenon begins under 975 nm CW excitation, when the energy is first absorbed by two nearby Yb^{3+} ions. This results with the promotion of sensitizers from their $^2F_{7/2}$–$^2F_{5/2}$ level. At this point, two simultaneous processes are happening. Due to the formation of coupled Yb^{3+} cluster state, another photon is absorbed and transferred towards $^1G_4$, from which 478 nm and 650 nm emissions occur. Also, there is a photon transferred from this level towards Eu^{3+} $^5D_1$, where after energy dissipation to $^5D_0$, several

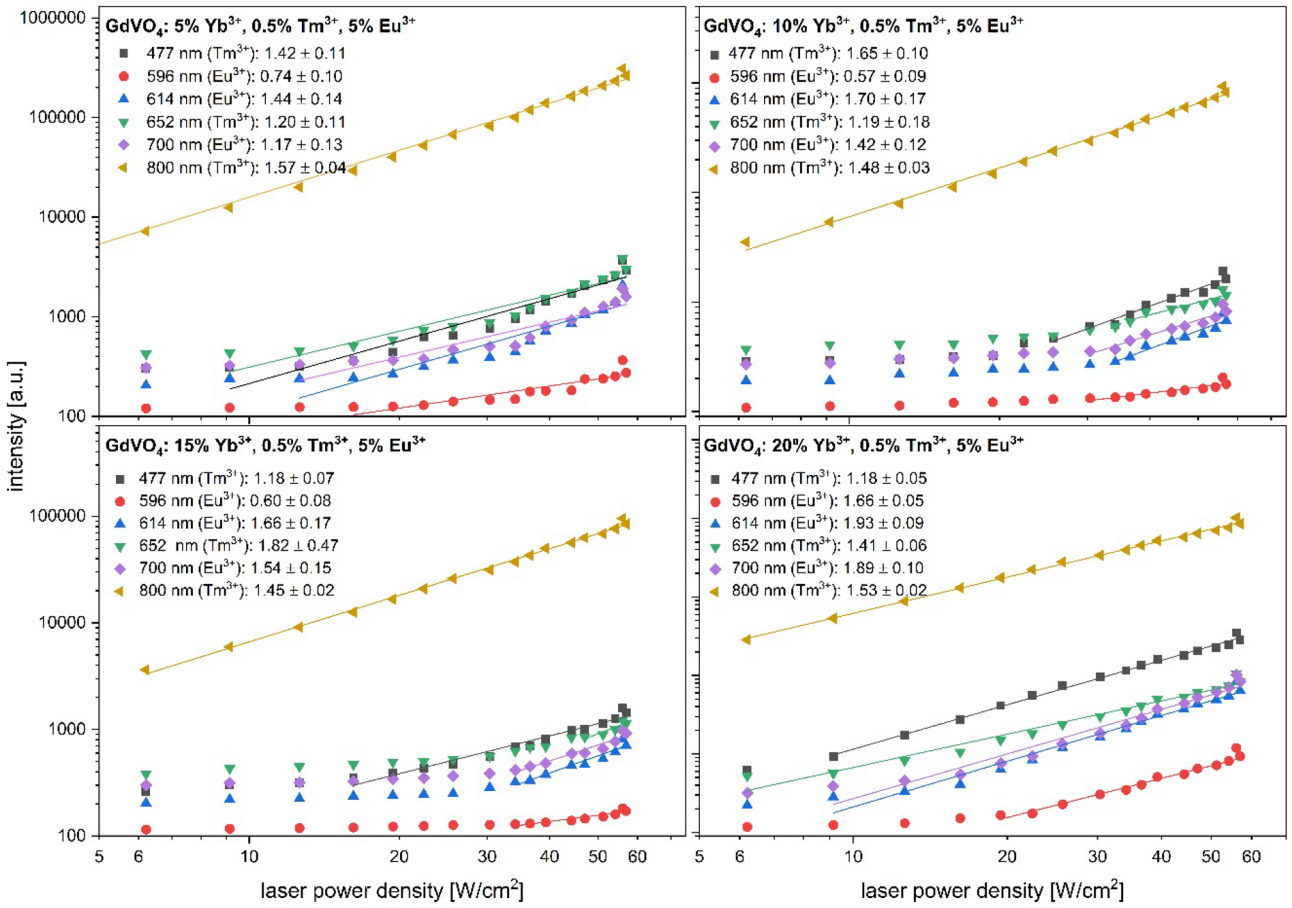

Figure 6. Laser power density studies for $GdVO_4$: x% Yb^{3+}, 0.5% Tm^{3+}, 5% Eu^{3+} samples recorded under CW 975 nm excitation.

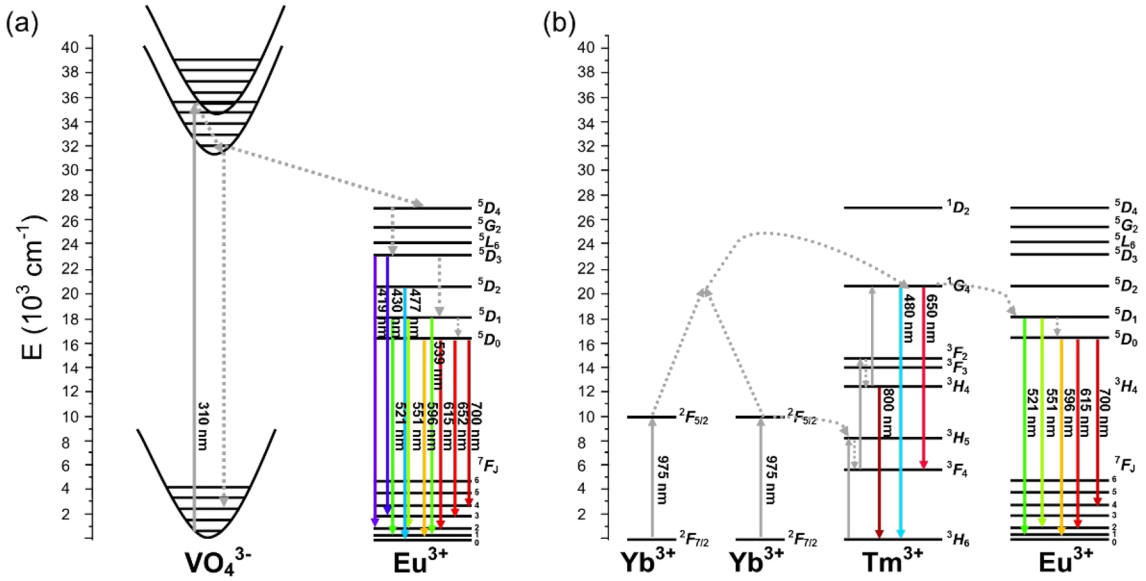

Figure 7. Energy level diagrams of Yb^{3+}, Tm^{3+} and Eu^{3+} ions and possible energy transfer (**a**) and UC (**b**) mechanism.

emissions associated with Eu^{3+} are observed in the spectrum. What is more, the Tm^{3+} $^3H_5$ is populated via photon transfer from Yb^{3+} $^2F_{5/2}$. After nonradiative relaxation to $^3H_4$, an 800 nm emission is observed.

Based on its pristine tunable luminescence properties, sample composed of $GdVO_4$: 20% Yb^{3+}, 0.5% Tm^{3+}, 5% Eu^{3+} was chosen for fibers preparation. Then luminescent fibers were used for paper modification and fabric production as an example of anti-counterfeiting application[43,44]. Regardless the medium, the outcoming luminescence color as well as its intensity remain unchanged. These properties recommend $GdVO_4$: 20% Yb^{3+}, 0.5% Tm^{3+}, 5% Eu^{3+} phosphor for anticounterfeiting applications performed in patent proposal submission. In Fig. 8, an actual luminescence color under different excitation sources is present.

Conclusions

To conclude, the pre-eminent, spectroscopic properties of $GdVO_4$: 20% Yb^{3+}, 0.5% Tm^{3+}, 5% Eu^{3+} define this material as the excellent one for anti-counterfeiting purposes. In our study, we investigated different Yb^{3+} concentration and its influence on structural and spectroscopic properties. With an increased sensitizer content, the upconversion luminescence is more intense whereas its color is tuned towards blue region of spectrum. What is more, in $Yb^{3+}/Tm^{3+}/Eu^{3+}$ system, $^1G_4 \rightarrow {}^3H_6$ and $^1G_4 \rightarrow {}^3F_4$ emissions result from twophoton excitation in terms of cooperative sensitization where two nearby Yb^{3+} ions are involved in IR excitation absorption process. Also, varied luminescence color under different sources of excitation qualified $GdVO_4$: 20% Yb^{3+}, 0.5% Tm^{3+}, 5% Eu^{3+}

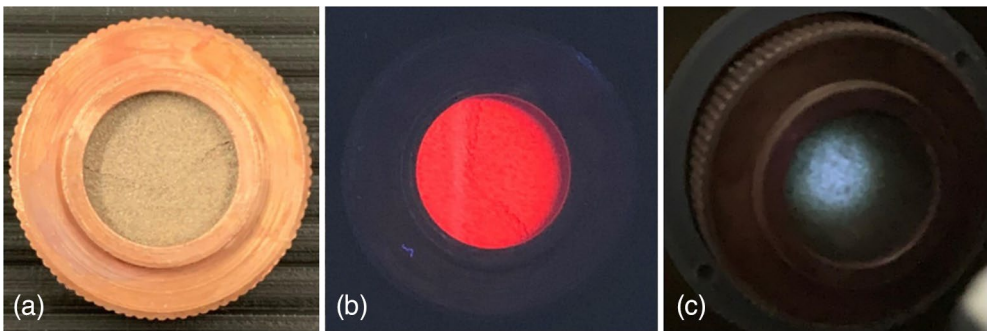

Figure 8. Actual images of $GdVO_4$: 20% Yb^{3+}, 0.5% Tm^{3+}, 5% Eu^{3+} powder in daylight (**a**), under 254 nm UV excitation (**b**) and 975 nm IR excitation (**c**).

phosphor for anticounterfeiting application. In applied cellulose medium, luminescence color and intensity remained unchanged in comparison to the phosphor in the powder state.

Data availability

The datasets generated during and analyzed during the current study are available from the corresponding author on reasonable request.

Received: 29 April 2023; Accepted: 24 June 2023
Published online: 04 July 2023

References

1. Shie, N. C., Hsieh, W. F. & Shy, J. T. Single frequency 1070 nm Nd:$GdVO_4$ laser using a volume Bragg grating. *Opt. Express.* **19**, 21109–21115 (2011).
2. Yi, S. S. *et al.* Photoluminescence behaviors of Eu-doped $GdVO_4$ thin film phosphors grown by pulsed laser ablation. *J. Alloys Compd.* **408–412**, 890–893 (2006).
3. Huang, S. J. *et al.* Luminescent $GdVO_4$:Eu^{3+} functionalized mesoporous silica nanoparticles for magnetic resonance imaging and drug delivery. *Dalt. Trans.* **42**, 6523–6530 (2013).
4. Przybylska, D., Grzyb, T., Erdman, A., Olejnik, K. & Szczeszak, A. Anti-counterfeiting system based on luminescent varnish enriched by NIR- excited nanoparticles for paper security. *Sci. Rep.* **12**, 19388 (2022).
5. Katumo, N., Li, K., Richards, B. S. & Howard, I. A. Dual-color dynamic anti-counterfeiting labels with persistent emission after visible excitation allowing smartphone authentication. *Sci. Rep.* **12**, 2100 (2022).
6. Moretti, E. *et al.* Luminescent Eu-doped $GdVO_4$ nanocrystals as optical markers for anti-counterfeiting purposes. *Chem. Pap.* **71**, 149–159 (2017).
7. Andresen, E. *et al.* Assessing the reproducibility and up-scaling of the synthesis of Er, Yb-doped NaY_F4-based upconverting nanoparticles and control of size, morphology, and optical properties. *Sci. Rep.* **13**, 2288 (2023).
8. Erdman, A., Kulpinski, P., Grzyb, T. & Lis, S. Preparation of multicolor luminescent cellulose fibers containing lanthanide doped inorganic nanomaterials. *J. Lumin.* **169**, 520–527 (2016).
9. Skwierczyńska, M., Runowski, M., Kulpiński, P. & Lis, S. Modification of cellulose fibers with inorganic luminescent nanoparticles based on lanthanide(III) ions. *Carbohydr. Polym.* **206**, 742–748 (2019).
10. Skwierczyńska, M. *et al.* Luminescent-magnetic cellulose fibers, modified with lanthanide-doped core/shell nanostructures. *ACS Omega* **3**, 10383–10390 (2018).
11. Tymiński, A., Śmiechowicz, E., Martín, I. R. & Grzyb, T. Ultraviolet- and near-infrared-excitable $LaPO_4$:Yb^{3+}/Tm^{3+}/Ln^{3+}(Ln = Eu, Tb) nanoparticles for luminescent fibers and optical thermometers. *ACS Appl. Nano Mater.* **3**, 6541–6551 (2020).
12. Shen, X., Hu, Q., Jin, Y. & Ge, M. Long-lived luminescence and photochromic cellulose acetate-based fiber: Preparation, characterization, and potential applications. *Cellulose* **30**, 2181–2195 (2023).
13. Yan, Y. *et al.* Effect of SDS on morphology tailoring of $GdVO_4$:Eu^{3+} powders under hydrothermal conditions in a wide pH range. *J. Alloys Compd.* **597**, 282–290 (2014).
14. Guo, J., Wang, W., Lin, H. & Liang, X. High-repetition-rate and high-power picosecond regenerative amplifier based on a single bulk Nd:$GdVO_4$ crystal. *High Power Laser Sci. Eng.* **7**, 1–7 (2019).
15. Gavrilovic´, T. V., Jovanovic´, D. J., Lojpur, V. & Dramic´anin, M. D. Multifunctional Eu^{3+}- and Er^{3+}/Yb^{3+}-doped $GdVO_4$ nanoparticles synthesized by reverse micelle method. *Sci. Rep.* **4**, 4209 (2014).
16. Tian, Y. Development of phosphors with high thermal stability and efficiency for phosphor-converted LEDs. *J. Solid State Light.* **1**, 1–15 (2014).
17. Wang, D. & Kodama, N. Visible quantum cutting through downconversion in $GdPO_4$:Tb^{3+} and $Sr_3Gd(PO_4)_3$:Tb^{3+}. *J. Solid State Chem.* **182**, 2219–2224 (2009).
18. Han, Q. *et al.* Tunable multicolor emission based on dual-mode luminescence Y_2O_3:Eu@SiO_2/Y_2O_3:Er(Tm/Yb) composite nanomaterials. *J. Lumin.* **241**, 118541 (2022).
19. Cui, S. *et al.* Tunable concentration-dependent upconversion and downconversion luminescence in $NaYF_4$: Yb^{3+}, Er^{3+}@ $NaYF_4$: Yb^{3+}, Nd^{3+} core-shell nanocrystals for a dual-mode anti-counterfeiting imaging application. *Opt. Lett.* **47**, 2814–28171 (2022).
20. Wanas, W., Abd El-Kaream, S. A., Ebrahim, S., Soliman, M. & Karim, M. Cancer bioimaging using dual mode luminescence of graphene/FA-ZnO nanocomposite based on novel green technique. *Sci. Rep.* **13**, 27 (2023).
21. Ayachi, F. *et al.* Dual-mode luminescence of Er3+/Yb3+ codoped $LnP_{0.5}V_{0.5}O_4$ (Ln=Y, Gd, La) for highly sensitive optical nanothermometry. *Mater. Today Chem.* **27**, 101352 (2023).
22. Marciniak, L., Bednarkiewicz, A. & Strek, W. Tuning of the up-conversion emission and sensitivity of luminescent thermometer in $LiLaP_4O_{12}$:Tm, Yb nanocrystals via E^{u3}+ dopants. *J. Lumin.* **184**, 179–184 (2017).
23. Jin, C. & Zhang, J. Upconversion luminescence of $Ca_2Gd_8(SiO_4)_6O_2$:Yb^{3+}-Tm^{3+}-Tb^{3+}/Eu^{3+} phosphors for optical temperature sensing. *Opt. Laser Technol.* **115**, 487–492 (2019).
24. Tymiński, A., Grzyb, T. & Lis, S. $REVO_4$-based nanomaterials (RE = Y, La, Gd, and Lu) as Hosts for Yb^{3+}/Ho^{3+}, Yb^{3+}/Er^{3+}, and Yb^{3+}/Tm^{3+} Ions: structural and up-conversion luminescence studies. *J. Am. Ceram. Soc.* **99**, 3300–3308 (2016).
25. Li, Y. *et al.* Growth phase diagram and upconversion luminescence properties of $NaLuF_4$:Yb^{3+}/Tm^{3+}/Gd^{3+} nanocrystals. *RSC Adv.* **7**, 44531–44536 (2017).
26. Liu, J. *et al.* A highly sensitive and selective nanosensor for near-infrared potassium imaging. *Sci. Adv.* **6**, 1–11 (2020).
27. Szczeszak, A. *et al.* Structural, spectroscopic, and magnetic properties of Eu^{3+}-doped $GdVO_4$ nanocrystals synthesized by a hydrothermal method. *Inorg. Chem.* **53**, 12243–12252 (2014).
28. Alammar, T., Cybinska, J., Campbell, P. S. & Mudring, A. V. Sonochemical synthesis of highly luminescent Ln_2O_3:Eu^{3+} (Y, La, Gd) nanocrystals. *J. Lumin.* **169**, 587–593 (2016).
29. Shannon, R. D. Revised effective ionic radii and systematic studies of interatomic distances in halides and chalcogenides. *Acta Crystallogr. Sect. A.* **32**, 751–767 (1976).
30. Xin, H., Lin, L. X., Wu, J. H. & Yan, B. Hydrothermal synthesis and multi-color photoluminescence of $GdVO_4$:Ln^{3+} (Ln = Sm, Dy, Er) sub-micrometer phosphors. *J. Mater. Sci. Mater. Electron.* **22**, 1330–1334 (2011).
31. Thakur, H. *et al.* Synthesis, structural analysis, upconversion luminescence and magnetic properties of Ho^{3+}/Yb^{3+} co-doped $GdVO_4$ nanophosphor. *Mater. Chem. Phys.* **253**, 123333 (2020).
32. Jovanović, D. J. *et al.* Synthesis, structure and spectroscopic properties of luminescent $GdVO_4$:Dy^{3+} and $DyVO_4$ particles. *Opt. Mater. (Amst)* **76**, 308–316 (2018).
33. Grzyb, T., Wecławiak, M. & Lis, S. Influence of nanocrystals size on the structural and luminescent properties of GdOF:Eu^{3+}. *J. Alloys Compd.* **539**, 82–89 (2012).
34. Zhao, J., Guo, C., Yu, J. & Yu, R. Spectroscopy properties of Eu^{3+} doped Ca $_9R(VO_4)_7$ (R=Bi, La, Gd and Y) phosphors by sol-gel method. *Opt. Laser Technol.* **45**, 62–68 (2013).

35. Behrh, G. K., Gautier, R., Latouche, C., Jobic, S. & Serier-Brault, H. Synthesis and photoluminescence properties of $Ca_2Ga_2SiO_7:Eu^{3+}$ red phosphors with an intense $^5D_0 \rightarrow {}^7F_4$ transition. *Inorg. Chem.* **55**, 9144–9146 (2016).
36. Choi, Y. I., Yoon, Y., Kang, J. G. & Sohn, Y. Photoluminescence imaging of Eu(III) and Tb(III)-embedded SiO_2 nanostructures. *J. Lumin.* **158**, 27–31 (2015).
37. Han, S. *et al.* Luminescence behavior of Eu^{3+} in silica glass containing $GdVO_4$: Eu nanocrystals. *J. Non. Cryst. Solids.* **532**, 119894 (2020).
38. Szczeszak, A. *et al.* Structural, spectroscopic, and magnetic properties of $Eu^{(3+)}$-doped $GdVO_4$ nanocrystals synthesized by a hydrothermal method. *Inorg. Chem.* **53**, 12243–12252 (2014).
39. Zhang, W. J. *et al.* Downshifting by energy transfer in Eu^{3+}/Yb^{3+} codoped $Ba_4La_6(SiO_4)_6O$ glass ceramics. *Phys. B Condens. Matter.* **508**, 22–26 (2017).
40. Quintanilla, M., Núñez, N. O., Cantelar, E., Ocaña, M. & Cussó, F. Tuning from blue to magenta the up-converted emissions of $YF_3:Tm^{3+}/Yb^{3+}$ nanocrystals. *Nanoscale* **3**, 1046–1052 (2011).
41. Gea, W., Xua, M., Shia, J., Zhua, J. & Li, Y. Highly temperature-sensitive and blue upconversion luminescence properties of $Bi_2Ti_2O_7:Tm^{3+}/Yb^{3+}$ nanofibers by electrospinning. *J. Chem. Eng.* **391**, 123546 (2020).
42. Liao, M. *et al.* Mechanisms of Yb^{3+} sensitization to Tm^{3+} for blue upconversion luminescence in fluorophosphate glass. *Mater. Lett.* **61**, 70–472 (2007).
43. Szczeszak, A. *et al.* P.438197 (2021).
44. Szczeszak, A. *et al.* P.438196 (2021).

Acknowledgements

This research was funded by scientific Grant LIDER (Grant No. 39/0141/L-9/17/NCBR/2018), The National Centre for Research and Development, Poland. We acknowledge Adrianna Nowak for her work in laboratory by phosphors' syntheses.

Author contributions

N.J.—Methodology, Investigation, Writing – Original Draft, Visualization ; J.Cz.—Writing – Review & Editing, Visualization; A.Sz.—Writing – Review & Editing, Supervision, Validation, Funding acquisition.

Competing interests

The authors declare no competing interests.

Additional information

Correspondence and requests for materials should be addressed to A.S.

Reprints and permissions information is available at www.nature.com/reprints.

Publisher's note Springer Nature remains neutral with regard to jurisdictional claims in published maps and institutional affiliations.

Open Access This article is licensed under a Creative Commons Attribution 4.0 International License, which permits use, sharing, adaptation, distribution and reproduction in any medium or format, as long as you give appropriate credit to the original author(s) and the source, provide a link to the Creative Commons licence, and indicate if changes were made. The images or other third party material in this article are included in the article's Creative Commons licence, unless indicated otherwise in a credit line to the material. If material is not included in the article's Creative Commons licence and your intended use is not permitted by statutory regulation or exceeds the permitted use, you will need to obtain permission directly from the copyright holder. To view a copy of this licence, visit http://creativecommons.org/licenses/by/4.0/.

© The Author(s) 2023